

Electrical Breakdown in a V_2O_3 device at the Insulator to Metal Transition

S. Guénon,^{1,*} S. Scharinger,² Siming Wang,^{1,3} J. G. Ramírez,¹ D. Koelle,² R. Kleiner,² and Ivan K. Schuller¹

¹*Department of Physics and Center for Advanced Nanoscience,
University of California-San Diego, La Jolla, California 92093, USA*

²*Physikalisches Institut and Center for Collective Quantum Phenomena in LISA⁺,
Universität Tübingen, Auf der Morgenstelle 14, D-72076 Tübingen, Germany*

³*Materials Science and Engineering Program, La Jolla, California 92093, USA*

(Dated: October 29, 2018)

We have measured the electrical properties of a V_2O_3 thin film micro bridge at the insulator metal transition (IMT). Discontinuous jumps to lower voltages in the current voltage characteristic (IV) followed by an approximately constant voltage progression for high currents indicate an electrical breakdown of the device. In addition, the IV curve shows hysteresis and a training effect, i.e. the subsequent IV loops are different from the first IV loop after thermal cycling. Low temperature scanning electron microscopy (LTSEM) reveals that the electrical breakdown over the whole device is caused by the formation of electro-thermal domains (ETDs), i.e. the current and temperature redistribution in the device. On the contrary, at the nanoscale, the electrical breakdown causes the IMT of individual domains. In a numerical model we considered these domains as a network of resistors and we were able to reproduce the electro-thermal breakdown as well as the hysteresis and the training effect in the IVs.

MAIN PAPER

Stoichiometric V_2O_3 is a strongly correlated material that undergoes a first order insulator to metal phase transition (IMT) from an antiferromagnetic insulating to a paramagnetic metallic phase. Because the IMT causes a change in the resistivity of several orders of magnitude novel devices based on the IMT and their applications are actively investigated [1] and it is in focus of current research whether there is a voltage driven IMT in strongly correlated materials [2–6]. If this hypothesis holds, a micro bridge fabricated of a strongly correlated material would experience a dielectric breakdown for high bias voltages. However, because of the large resistivity change, self-heating in such a device can be strong enough to cause an electro-thermal breakdown, i.e. an current and temperature redistribution [7, 8]. In order to investigate the electrical breakdown of a V_2O_3 micro bridge, we used a very unique low temperature scanning electron microscope (LTSEM) to image the metallic and insulating phases and developed a numerical model to simulate the electrical device properties. Here we show that the electrical breakdown over the whole device is due to the formation of electro-thermal domains (ETDs), and that the distribution in the IMT temperature as well as the hysteresis in the RT of domains at the nanoscale are significantly influencing the current voltage characteristic (IV).

The V_2O_3 film was grown by rf-sputtering on a r-cut sapphire substrate at a temperature of approximately 750 °C. XRD revealed that the polycrystalline film grows textured under these conditions. Optical contact lithography was used for patterning. A 200 μm wide V_2O_3 bridge was etched using reactive ion etching and gold

electrodes were evaporated on top, refer to Fig. 1 (a) for an SEM image of the device.

The same experimental set up was used for LTSEM imaging and IV characterization. The LTSEM is a conventional, state of the art SEM equipped with a LN₂-cryostat. The sample is mounted in a vacuum on a cold plate and the sample temperature can be varied from room temperature to approximately 80 K. Due to the large working distance required by the IR-shielding of the cryostat the smallest spot size of the electron beam is about 300 nm. A Keithley 2400 current source and a conventional preamplifier with a National Instruments measurement card were used for the two point electrical measurements.

To acquire a LTSEM image, the sample is scanned with a blanked electron beam and the electric response ΔV of a simultaneously applied four probe or two probe measurement is mapped in a so called voltage image of the sample [9, 10].

We have measured the current-voltage characteristics of a 200 μm wide and 10 μm long V_2O_3 bridge (Fig. 1a) for the base temperatures $T_b = 145$ K and $T_b = 155$ K, respectively. Due to the IMT there is a resistance change by more than three orders of magnitude in a 20 K temperature interval (Fig. 1b) and a pronounced hysteresis, i.e. the heating curve is shifted to higher temperatures by approximately 5 K.

To ensure that the V_2O_3 film was completely in the insulating state the device temperature was reduced to approximately 80 K and then heated to the intended base temperature before electrical measurements were started. In the following, we refer to this procedure as “thermal cycling”.

Fig. 1c shows an IV of the pristine device (after thermal cycling) acquired at a base temperature $T_b=145$ K.

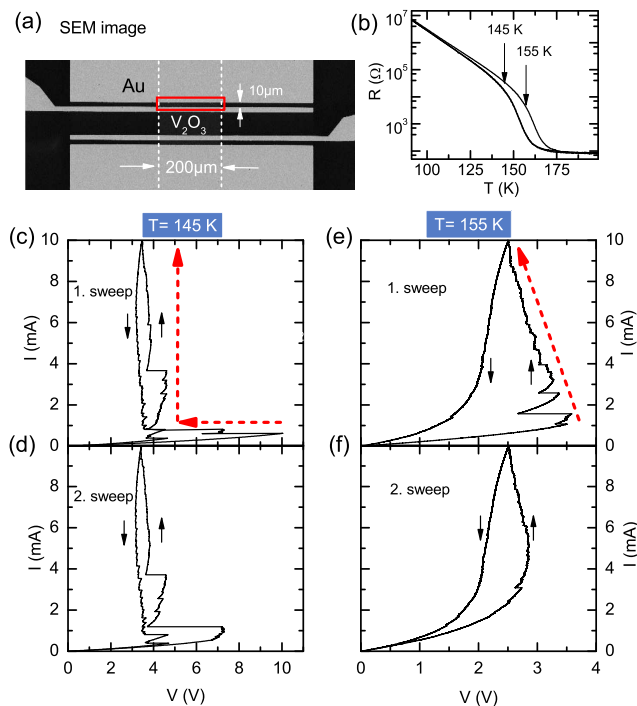


FIG. 1. (Color online) Electrical breakdown. (a) SEM image of the device. The area under investigation is indicated by a red rectangle. A $200\ \mu\text{m}$ wide V_2O_3 stripe runs vertically indicated by two white dashed lines. The two gold electrodes at the top form a $10\ \mu\text{m}$ wide gap. The current flows between those two electrodes vertically. (b) Temperature dependence of the device resistance. Current voltage characteristics (IVs) at two different base temperatures. The black arrows indicate the sweep direction. The overall progression of the electrical breakdown is indicated by red dashed arrows. (c) and (e) are IVs of the pristine device after cooling to 80 K. (d) and (f) are subsequent IVs to (c) and (e), respectively.

Starting at the origin of the graph, the IV shows an almost linear dependence with a slight upwards bent. At a current value of $0.6\ \text{mA}$ there is a jump from $10\ \text{V}$ to $7\ \text{V}$ followed by several small jumps and a big jump to $3.8\ \text{V}$. The curve continues almost vertically with a positive slope and several sawtooth like discontinuities of different sizes. The down sweep curve is different from the up sweep, i.e. there is a hysteresis. Immediately after the first IV curve, without changing the base temperature, a second IV was acquired (Fig. 1f). Note, that the IV of the second sweep is very similar to the first one except that the maximum voltage is significantly reduced. When the device is thermally cycled, the old state (first sweep) is restored. Hence, there is a training effect. The curve acquired at the first sweep at $155\ \text{K}$ (Fig. 1e) is different from the one at $145\ \text{K}$. Starting at the origin, the IV is almost linear. After $1\ \text{mA}$ and $3.5\ \text{V}$ it progresses with a negative slope and saw tooth like discontinuities of different sizes. The down sweep curve is rounded with some very small discontinuities and the hysteresis is much

more pronounced than at $145\ \text{K}$. In the second IV (Fig. 1f) the down sweep is similar to the down sweep of the first IV, but the up sweep curve is round and there are only a few small discontinuities. A comparison between the IV of the first and second sweep reveals, that the training effect at $155\ \text{K}$ leads to a qualitative change of the up sweep curve. The consecutive IVs do not change significantly after the second sweep at both base temperatures. Moreover, we have observed that the details of the IV depend on the sweep velocity. If the current is swept faster, there are more and smaller jumps, but the overall shape of the IV stays the same.

At $T_b=145\ \text{K}$ a big jump in the IV followed by a vertical progression indicates an electrical breakdown of the device. The diagonal progression with a negative slope and small jumps in the first IV at $T_b=155\ \text{K}$ implies that the electrical breakdown now evolves via stable intermediate states. From the hysteresis in the IVs and the training effect it can be inferred that there is a memory effect in the V_2O_3 device, i.e. the device properties depend on its history. Similar effects were reported in VO_2 devices [11]. The slight influence of the sweep velocity on the IV might be caused by a slowed down relaxation of a small fraction of the film due to the spread in the IMT temperatures of individual domains [12].

The LTSEM images at a base temperature of $145\ \text{K}$, are discussed below [Fig. 2]. In order to relate the images to the current voltage characteristic, the IV of the second sweep in Fig. 1 is depicted. We have discovered that the imaging process changes somewhat the resistance of the device. In Fig. 2 (a) the bias points before and after imaging are indicated by red arrows. In the images at bias points below the first big jump (b-e) a cluster of dots appears in an approximately $10\ \mu\text{m}$ wide section of the device indicated by a dashed yellow rectangle in image (f). In the images at bias points above the first jump (f-k) a bright stripe appears whose width increases with increasing currents.

A series of LTSEM images acquired at a base temperature of $155\ \text{K}$ are shown in Fig. 3. If the bias is increased, submicron sized dots of different brightness appear. The majority of them is clustered in the same small section of the device, where at $T_b = 145\ \text{K}$ the electrical breakdown occurs. For increasing currents the density of these dots increases and they merge. When an imaging scan is repeated at the same bias current, the images look more or less the same and additional bright spots appear at different positions.

In the supplement, the LTSEM response ΔV to the modulated electron beam is estimated. This shows that ΔV is proportional to the temperature derivative of the conductivity close to the electron probe $\frac{d\sigma}{dT}$. Because $\frac{d\sigma}{dT}$ in the insulating phase is several orders of magnitude smaller than in the metallic phase, a large response ΔV is predominately caused by the metallic domains. The bright sub microns sized spots, which saturate the signal in the

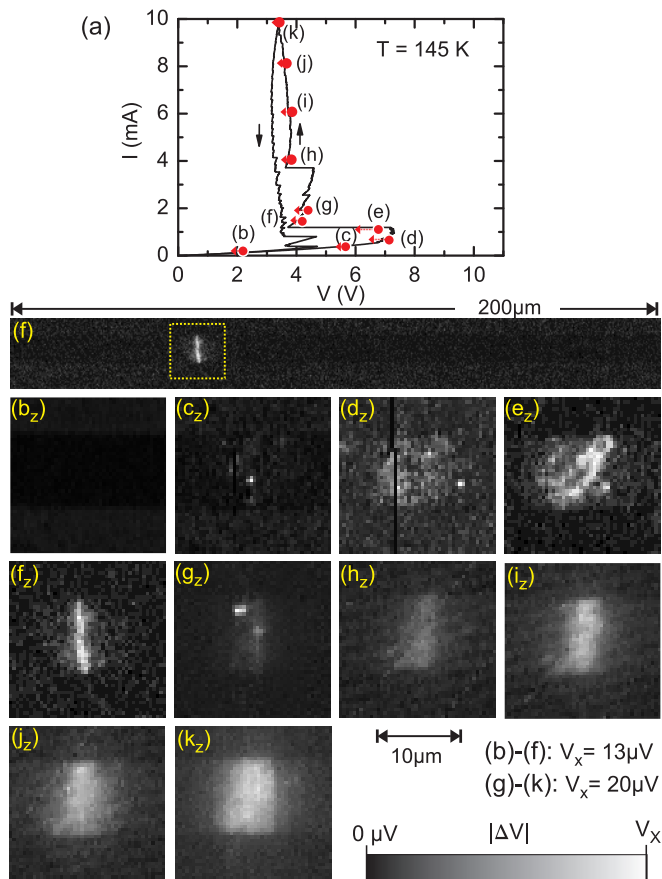


FIG. 2. (Color online) LTSEM voltage-images acquired at different bias currents at a base temperature of 145 K. (a) IV of figure 1 (c). The start points and the end points before and after imaging are indicated by red arrows. (f) image of the entire device. ($b_z - k_z$) images with a reduced field of view (indicated by a yellow dashed rectangle in f).

LTSEM images, might be due to current redistribution. In the LTSEM image series at $T_b=145$ K (Fig. 2) a metallic filament appears (electro-thermal domains) like reported in VO_2 devices [7, 8]. In the $T_b=155$ K series no filament appears, but the device becomes gradually metallic in a small section of the device when the current is increased.

In order to investigate how the IMT transition of domains at the nanoscale are influencing the electrical breakdown, we have developed a numerical model (similar to the one used in [13]), in which we represent domains with different IMT temperatures by a 20×400 resistor network (see supplement). For each domain the same hysteresis ΔT_c in the RT-dependence was assumed, but for the IMT temperatures T_c a Gaussian distribution was used (Fig. 4 a). The hysteresis as well as the median and the standard deviation of this Gaussian distribution were obtained by optimizing the simulated RT-curve with respect to the measured RT (Fig. 4 b). Then these values ($\Delta T_c = 8$ K, $T_c = 163$ K and $\text{RMSD} \approx 3.16$) were used

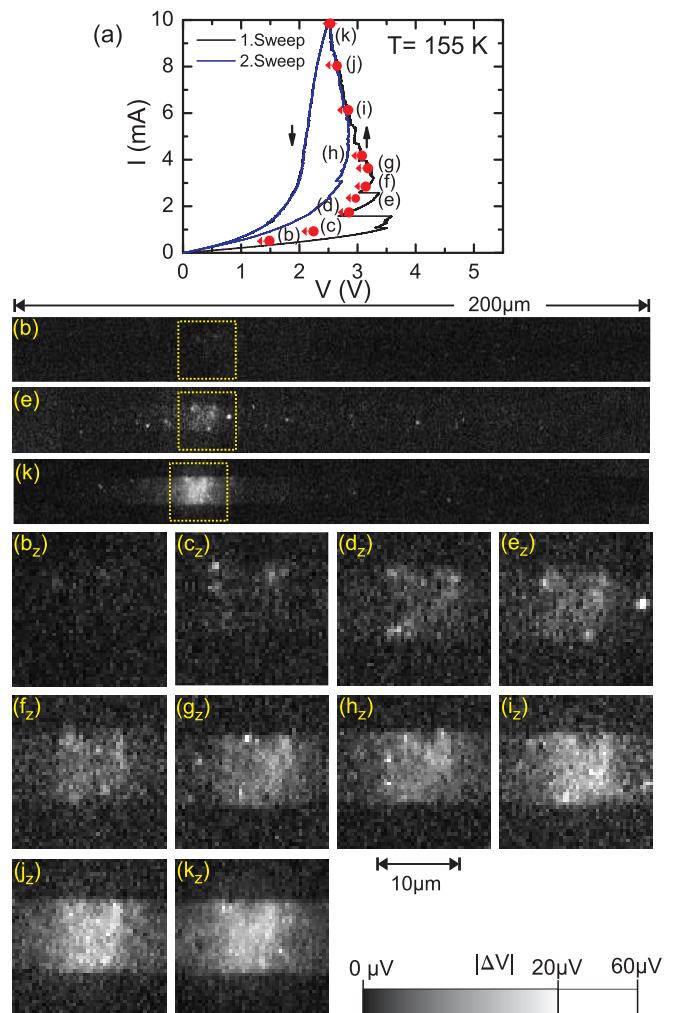


FIG. 3. (Color online) LTSEM voltage images acquired at different bias currents at a base temperature of 155 K. (a) IVs of figure 1 (e-f). The start points and the end points before and after imaging are indicated by red arrows. (b, e, and k) images of the entire device. ($b_z - k_z$) images with a reduced field of view (indicated by a yellow dashed rectangle in b,e, and k).

to simulated the IVs as well as the temperature, current and voltage distributions for the base temperatures $T_b = 145$ K (Fig. 4 c-e) and $T_b = 155$ K (Fig. 4 f-h). The simulated current and voltage distributions are shown in the supplement.

The hysteresis and the training effect in the IVs could be reproduced. The simulation at $T_b = 145$ K shows the formation electro-thermal domains like in the LTSEM-images (Fig. 2). There are significant differences between the simulation and measurements at $T_b = 155$ K: The simulation clearly shows the formation of electro-thermal domains (filaments), while the IV progresses vertically (Fig. 4 f-g). In the LTSLM images no filament appears and the IV progresses diagonally (Fig. 3).

Conclusion: The hysteresis and the training effect in the

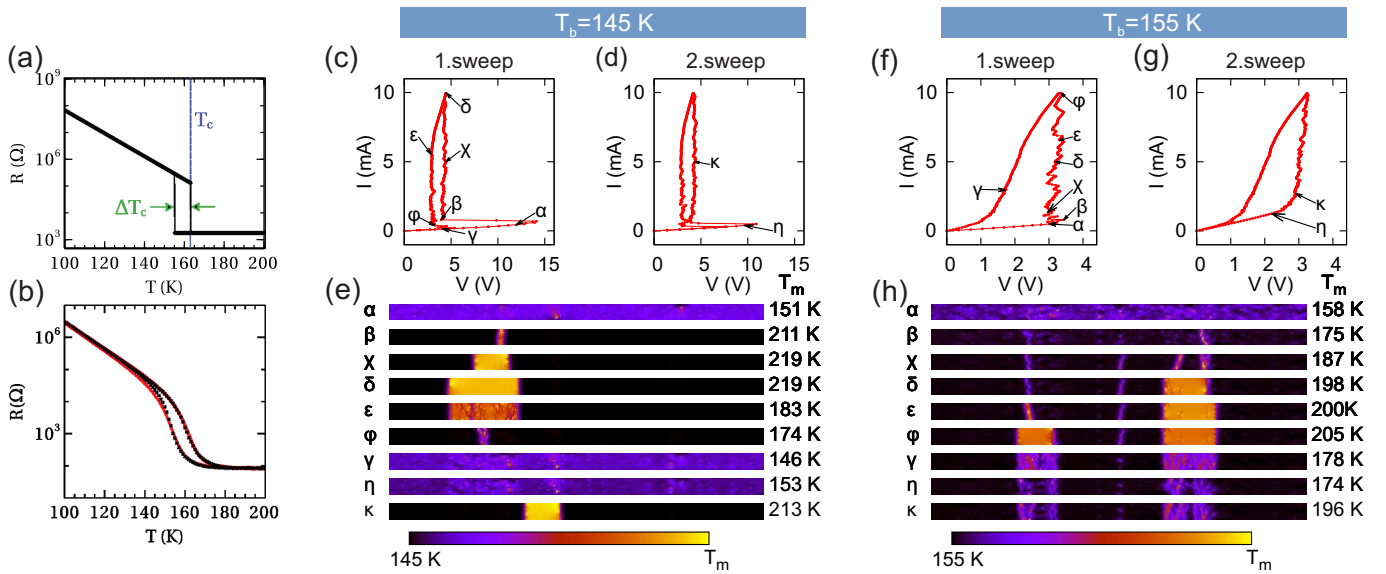


FIG. 4. (Color Online) Numerical model. (a) Assumed resistance vs. temperature dependence for an individual domain. T_c denotes the IMT temperature (heating curve). ΔT_c is the temperature difference by which the cooling curve is shifted. (b) Simulated resistance vs. temperature dependence. The crosses are simulated points and the continuous line is the measured curve. (c) Simulated IV of the pristine device (base temperature $T_b = 145$ K). (d) Consecutive IV. (e) Temperature distributions in the device at different bias points (marked in (c) and (d) with Greek letters). (f) Simulated IV of the pristine device (base temperature $T_b = 155$ K). (g) Consecutive IV. (h) Temperature distributions in the device at different bias points (marked in (f) and (g) with Greek letters).

IV are the results of the RT hysteresis as well as the distribution of IMT temperatures of nanoscaled domains in the polycrystalline thin film. It is plausible that the RT hysteresis originates from the structural bistability reported earlier [14–16] and the spread in the transition temperatures is most likely caused by differences in the strain in the polycrystalline film [12, 17].

At a base temperature of 145 K the overall IV and the ETDs (filaments) depicted in Fig. 2 (f-k) were reproduced in the simulation, clearly indicating an electro-thermal breakdown of the device.

On the contrary, at a base temperature of 155 K the electrical breakdown, with the small metallic domains clustered in a small section of the device and the diagonal progression of the IV (Fig. 3), is very atypical for an electro-thermal breakdown. Generally, in a system, where the electro-thermal bistability is caused by a large decrease in the device resistance with increasing temperature the electro-thermal domain walls are parallel to the current direction, i.e. in the sample under investigation, electro-thermal domains have always the shape of a filament. After electro-thermal domains have nucleated, the IV progresses vertically, while the hot electro-thermal domains increase in size [18, 19] (see also the supplement). We provide three different explanations for the electrical breakdown via stable intermediate states at a base temperature of 155 K. First, it is possible to stabilize an electro-thermal bistable device in intermediate states by using a load resistor, which forces the IV to progress

along a diagonal load line during the electro-thermal breakdown [20]. The device under test has a relatively high contact resistance of approximately 80Ω . If one assumes that this contact resistance is nonohmic and has a tunneling characteristic, the sawtooth like discontinuities and the diagonal progression of the IV at 155 K can be explained. Second, an intrinsic shunting of small domains above a certain threshold voltage that could be caused by Landau-Zener tunneling [2–5] might have a similar effect. Third, in a theoretical model considering voltage induced switching two different electrical breakdown mechanism were predicted - bolt like and percolative switching [21]. According to this results one might interpret the electrical breakdown at a base temperature of 145 K as bolt like and at 155 K as percolative switching. In this model thermal coupling within the thin film and to the substrate was not considered. When we explicitly included voltage induced switching in our model, we were never able to observe percolative switching, but we always observed the formation of a filament. The only effect was to shift the thermal breakdown to lower voltages. This is quite plausible, because the sample heating effects occur at lower voltages, in this case. From the simulated voltage distribution in the supplement a threshold voltage for a dielectric breakdown below 20 kV/cm can be inferred. This value would be very small. Therefore, we consider the first explanation as the most likely scenario.

SUPPLEMENT

Self-heating, electrothermal bistability and the formation of electrothermal domains (ETDs)

Self-heating, thermal bistability and the formation of electrothermal domains (ETDs), are discussed in the following section. The primary cause for these phenomena is a strong change in the resistivity vs. temperature characteristic of the material used for the device under investigation. These phenomena can be observed in large number of different kind of devices: There is the hot-spot in a superconducting microbridge [19, 22, 23], the pinch caused by thermal breakdown in a negative temperature coefficient thermistor (NTC) [24, 25], the domains in a two valley semi-conductor used in a Gunn-diode [18], the hot spot in a large BSCCO-mesa used as a THz-emitter [26–29] or the filaments in a VO_2 device [7, 30] at the metal-insulator transition, to name only a few examples. In the following, only the basics of this topic necessary to understand the supplemented paper are provided. A more elaborate discussion can be found in the review articles [18, 19].

Self-heating

In a device with finite electrical resistance the Joule heating leads to a rise in the device temperature. This temperature increase depends on the thermal coupling of the device to the environment. If the device resistance is temperature dependent (as it is usually the case), this self-heating effect causes a deviation in the current voltage characteristic (IV) from the linear (Ohmic) progression. In other words, there will be bending in the IV. If the device resistance changes strongly with temperature, this bending can be very pronounced as it is demonstrated in the following.

If the temperature dependence of the device resistance and the thermal coupling are known, and a uniform temperature distribution is assumed the IV can be parameterized using a method similar to the graphical method described in [31].

The excess temperature ϑ of the device is determined by Ohm's law and Newton's law of cooling:

$$V = R(\vartheta) I; \quad V I = A(\vartheta), \quad (1)$$

where $A(\vartheta)$ is the heat transfer coefficient. The parameterization of the IV is

$$V = \sqrt{R(\vartheta) A(\vartheta)} \quad \text{and} \quad I = \sqrt{\frac{A(\vartheta)}{R(\vartheta)}}. \quad (2)$$

This method is now applied to the V_2O_3 device discussed in the article. On the assumption that the thermal conductance of the device is solely determined by the sapphire substrate and "edge cooling" can be neglected the

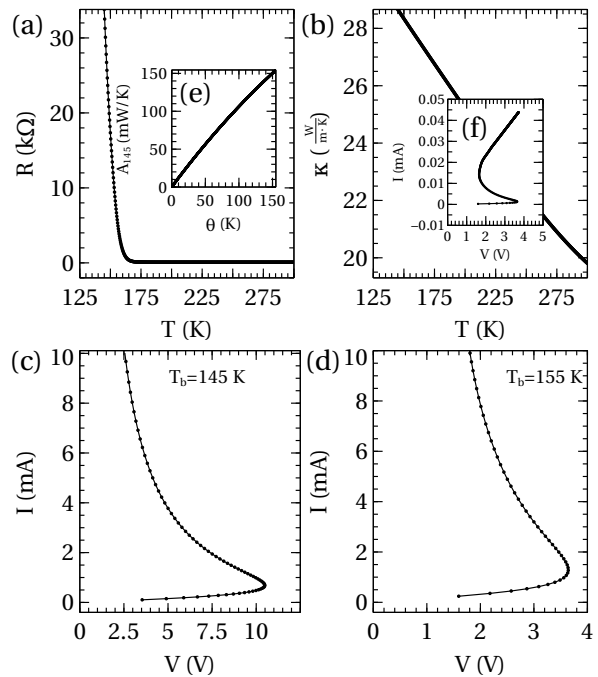


FIG. 5. Influence of self-heating on the current voltage characteristic of the V_2O_3 device: (a) Temperature dependence of the device resistance. (b) Thermal conductivity of sapphire vs. temperature. (c) and (d) calculated current voltage characteristics of the device, assuming a homogenous temperature distribution. The base temperatures are $T_b = 145 \text{ K}$ and $T_b = 155 \text{ K}$, respectively. Inset (e) heat transfer coefficient via the sapphire substrate vs. excess temperature θ assuming a base temperature $T_b = 145 \text{ K}$. Inset (f) IV of figure (d) at a larger scale.

heat transfer coefficient can be calculated using the thermal conductivity κ of sapphire

$$A(\vartheta) = \frac{LW}{H} \int_{T_b}^{T_b+\vartheta} \kappa(T) dT \quad (3)$$

Here L is the length, W the width and H the height of the device and T_b is the base temperature.

Figure 5 c) and d) show the parameterized IV at the base temperature $T_b = 145 \text{ K}$ and $T_b = 155 \text{ K}$, respectively. $H = 0.5 \text{ mm}$, $W = 200 \mu\text{m}$ and $L = 20 \mu\text{m}$ were used. For current values below 1 mA the calculated IVs of this supplement are similar to the measured IVs presented in the main paper. The IV with a large current scale (inset [Fig. 5(f)]) has a very pronounced S-shaped characteristic.

Electrothermal Bistability

In the preceding section it was demonstrated that in a device, with a strong resistance decrease in a small temperature interval, self-heating leads to an S-shaped IV curve, *cf.* [Fig. 5(f)]. If a voltage source is used to

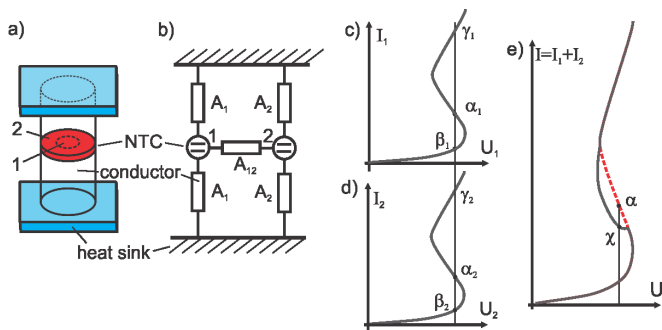


FIG. 6. Formation of electrothermal domains, according to [24]: (a) NTC clamped between two metal pins. (b) Thermal equivalent circuit: A_1 and A_2 denote the thermal coupling to the heat sink and A_{12} the thermal cross coupling, respectively. (c) and (d) IV curve corresponding to the area 1 and area 2 of the device. (e) IV of the whole device.

bias such a device, then the system is (electrothermally) bistable, i.e. there exists a bias interval in which the system can rest in two different bias states: The one state has a low bias current and a low device temperature (denoted in 6 (c) and (d) with β_1 and β_2), while the other state has a high bias current and a high device temperature (denoted in 6 (c) and (d) with γ_1 and γ_2). Note, that for a device with a strong increase in resistivity the self-heating is causing an N-shaped IV and voltage and currents are changing their roles, but this supplement is restricted on the case with an S-shaped IV.

Formation of Electrothermal Domains

Electrothermal domains can form in a device with weak thermal coupling between different parts. According to [32] one of the first publications in the field of ETDs was the work of E. Spenke on the thermal breakdown of negative temperature coefficient thermistors (NTCs) [24, 25]. He discussed a NTC disk fixed between two metal pins, which are in contact with a thermal reservoir at a constant temperature, [Fig. 6(a)]. Note, that the resistance of the pins and the thermal reservoir is considerably smaller than the resistance of the disk. In a ‘‘Gedankenexperiment’’, E. Spenke divided the NTC-disk into two domains, or in other words he considered the disk consisting of two NTCs in parallel, which are thermally coupled via the metallic pins. He inferred that the system (under current bias) can stabilize itself in the bias interval of negative differential resistance, if one of those NTCs switches to a bias point in the IV that corresponds to a high bias current and high temperature (for instance bias point γ_1) and the other NTC switches to a bias point with low current and low temperature (for instance bias point β_2). This is equivalent to the formation of two areas with different current density and temper-

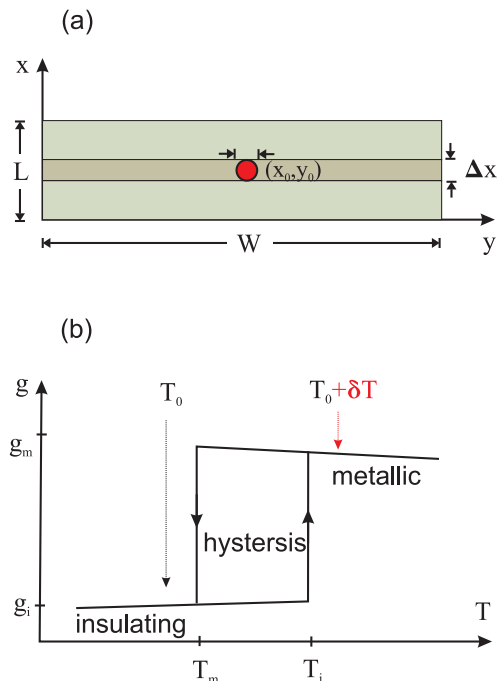


FIG. 7. a) Scheme of the device under investigation (top view), b) sketch of the specific conductivity vs. temperature.

ature, which are called electrothermal domains (ETDs). Note, only if the ETD walls are parallel to the current direction, the ETDs can be considered as parallel resistors and the argumentation of the ‘‘Gedankenexperiment’’ can be applied.

The formation of the electrothermal domains is causing a kink or a discontinuity in the IV. If the S-shape in the IV of a device with uniform temperature distribution is very pronounced than this discontinuity is very pronounced, too. After the formation of the ETDs the IV progresses almost vertically indicating that an increase of the current is increasing the size of the ‘‘hot’’ electrothermal domain with a high current density while the voltage over the device stays constant.

Low temperature scanning electron microscopy (LTSEM)

In the following we derive a relation between the LTSEM voltage signal $\Delta V(x_0, y_0)$ and the local conductance per area g of the V_2O_3 sample. In LTSEM a periodically blanked focused electron beam (using $f_b = 13.3$ kHz, acceleration voltage 10 kV, beam current 100 pA), is scanned across the sample surface in the (x, y) -plane. When the electron beam is positioned at coordinates (x_0, y_0) , it causes local heating and thus local changes in temperature-dependent parameters such as the local conductivity of the junction. This can be detected by means of lock-in technique as a beam-induced change

$\Delta V(x_0, y_0)$ of the voltage V across the junction, which is biased at a constant current I . The beam current also adds to the bias current density in the beam spot around

(x_0, y_0) . For measurements reported here, the beam current density is several orders of magnitude smaller than the typical transport current densities. Therefore, this effect will be ignored here.

If the electron beam is on, the local temperature increases by δT resulting in a temperature distribution $T(x - x_0, y - y_0) = T_0 + \delta T(x - x_0, y - y_0)$, where T_0 is the local temperature of the undisturbed junction. The temperature profile created by the beam typically has Gaussian shape

$$\delta T(x - x_0, y - y_0) = \Delta T \exp \left\{ -\frac{(x - x_0)^2 + (y - y_0)^2}{2\sigma^2} \right\}, \quad (4)$$

and $\Delta T \approx 0.1 - 1 \text{ K}$ and $\sigma \approx 0.3 - 2 \mu\text{m}$.

The geometry of the V_2O_3 device is a microbridge of length L along x , with a width W along y and a thickness D along z [Fig. 7 (a)]. Along z the incident electron beam heats the bridge almost homogeneously and we assume that the sample specific conductivity $g(x, y)$ does not depend on z . The bias current is applied in x direction. Further, since $W \gg L$ we assume that the currents inside the bridge strictly flow in x direction, i. e. we neglect voltage drops in y direction and current redistribution effects. With an electron beam illuminating a spot at the position (x_0, y_0) the beam induced voltage change is given by

$$\Delta V(x_0, y_0) = I(R_{\text{on}} - R_{\text{off}}), \quad (5)$$

where I is the total device current and $R_{\text{on/off}}$ is the resistance when the laser beam is on or off, respectively. We divide the device in N slabs oriented in the (y, z) plane with thickness Δx . The i -th slab with the coordinate x_i has the conductance G_i and the electron beam causes a small change in conductance δG_i . The device resistance for the electron beam off state can be written as $R_{\text{off}} =$

$\sum_{i=1}^N \frac{1}{G_i}$ and using a Taylor expansion

$$R_{\text{on}} = \sum_{i=1}^N \frac{1}{G_i + \delta G_i} \approx \sum_{i=1}^N \frac{1}{G_i} - \sum_{i=1}^N \frac{\delta G_i}{G_i^2} \quad (6)$$

From [5] and [6] follows

$$\Delta V(x_0, y_0) = -I \sum_{i=1}^N \frac{\delta G_i}{G_i^2} \quad (7)$$

We approximate the conductance of the i -th slab by averaging over the device

$$G_i \approx \frac{L}{\Delta x R_{\text{off}}}. \quad (8)$$

δG_i can be written as

$$\delta G_i = \frac{D}{\Delta x} \int_0^W \delta g(x_i, y, x_0, y_0) dy, \quad (9)$$

where $\delta g(x, y, x_0, y_0)$ is the local change of conductivity cause by an electron beam illuminating a spot at the position (x_0, y_0) .

We obtain for the beam induced voltage change

$$\Delta V(x_0, y_0) = - \sum_{i=0}^N \int_0^W \frac{I D}{L^2} R_{\text{off}}^2 \delta g(x_i, y, x_0, y_0) \Delta x dy = - \frac{I D}{L^2} R_{\text{off}}^2 \int_A \delta g(x, y, x_0, y_0) d(x, y) \quad (10)$$

The quantity to be evaluated further is $\int_A \delta g(x, y) d(x, y)$. In analogy with the assumed $R(T)$ dependence of an individual domain, see inset in [Fig. 5] of the main paper, we consider $g(x, y)$ of the domain as a function of T , which is characterized by three regions, see Fig. [7 (b)]. At temperatures T_0 far away from the insulation-to-metal transition (IMT) $g(x, y, T_0)$ is a unique function with g_i for the insulating state and g_m for the metallic state, respectively. At the

IMT the curve is hysteretic.

The e-beam induced change in conductance of an individual domain is qualitatively discussed in the following: T_0 is the temperature of the domain when the e-beam is off and δT is the temperature increase of the domain when the e-beam is on. According to [Fig. 7], if $T_0 > T_i$ (where T_i is the insulator to metal transition temperature) the change of the domain conductance is proportional to the slope $\frac{dg_m}{dT}$. If $T_0 < T_i$ and

$T_0 + \delta T < T_i$, the change of the domain conductance is proportional to the slope $\frac{dg_i}{dT}$ at T_0 . If $T_0 < T_i$ and $T_i < T_0 + \delta T$, the illumination with the electron beam causes an irreversible switching of the domain. This mechanism explains why the LTSEM imaging process is influencing the bias over the device as discussed in the main paper. After the domain has switched the beam induced change of the conductance is proportional to $\frac{dg_m}{dT}$. Finally, if $T_0 < T_m$ (where T_m is the metal to insulator transition temperature) and $T_i < T_0 + \delta T$, the

domain switches reversible between the insulating and the metallic state and the beam induced change of the domain conductance is proportional to $g_m - g_i \approx g_m$. Due to the lock-in technique this response can be detected in LTSEM in contrast to the irreversible switching. To summarize, there are three different response mechanism of an individual domain: Metallic, insulating and the reversible switching, which is denoted with the index h (for hysteresis) in the following.

Because the device temperature locally varies and different domains have different IMT temperatures, the device is divided in three areas $A = A_m + A_i + A_h$. Note, that the areas are not necessarily connected. For instance the device could consist of small metallic “puddles” embedded in an insulating matrix.

We rewrite $\int_A \delta g(x, y) d(x, y)$ as

$$\int_A \delta g(x, y) d(x, y) = \int_{A_m} \left[\frac{dg_m(x, y)}{dT} \Big|_{T_0} \delta T(x - x_0, y - y_0) \right] d(x, y) \quad (11)$$

$$+ \int_{A_i} \left[\frac{dg_i(x, y)}{dT} \Big|_{T_0} \delta T(x - x_0, y - y_0) \right] d(x, y) + \int_{A_h} [g_m(x, y) - g_i(x, y)] d(x, y).$$

The first term on the right hand side represents the regions of the sample which remains in the metallic (g_m) state and the second term represents domains that remain in the insulating state (g_i). The third term represents the domains, which reversibly switch between the insulating and the metallic state upon illumination. We may assume that N domains in a radius $\approx \sigma$ switch between the insulating and the metallic state. Let the area of the domain n be A_n . Then the third term reduces to $\sum_n A_n [g_m(T_m) - g_i(T_i)] \Theta(|\vec{r}_0 - \vec{r}_n|/\sigma)$, where \vec{r}_0 is a vector to point (x_0, y_0) and \vec{r}_n points to the center of the domain n . $\Theta(\xi)$ shall be 1 if $\xi < 1$ and 0 otherwise. If σ^2 is on the order of or smaller than A_n the domains which switch will be clearly distinguishable and $N = 0$ or 1. For

$\sigma^2 \gg A_n$ and not well separated switching domains one will see some blurred signal where the switching domains cannot be resolved clearly.

In the following we calculate and discuss the expected different responses of Eq. (11) for a device at 145 K at a bias 10 mA and 3.5 V which corresponds to image k in Fig. [3] of the main paper. For the insulating phase g_i and $\frac{dg_i}{dT}$ can be established by means of the inset in Fig. [5] of the main paper. At $T = 145$ K we get $g_i \approx 26.6 \frac{1}{\Omega \text{ m}}$ and $\frac{dg_i}{dT} \approx 1.37 \frac{1}{\Omega \text{ K m}}$. Because the device we discussed in the main paper has a high contact resistance, we used a four-terminal measurement on a device with comparable V_2O_3 thin film properties to determine $g_m \approx 1.43 \cdot 10^5 \frac{1}{\Omega \text{ m}}$ and $\frac{dg_m}{dT} \approx -310 \frac{1}{\Omega \text{ K m}}$.

For the beam induced voltage change due to switching of domains we finally find

$$\Delta V_h(x_0, y_0) \approx -IR_{\text{off}}^2 \frac{D}{L^2} \sum_n A_n g_m(T_0) \Theta(|\vec{r}_0 - \vec{r}_n|/\sigma) \quad (12)$$

$$\approx -0.05 \text{ V}, \quad (13)$$

with $N = 1$ and $A_n = (0.5 \times 0.5) \mu\text{m}^2$.

This expected value exceeds our measured signal by several orders of magnitude and is even higher for lower bias currents. According to the simulations of temperature distribution [Fig. 6-7 of the main paper], the local temperature within an ETD ($T_{\text{ETD}} \approx 210$ K) is clearly

above T_i . Furthermore, since the electron beam generates a local increase in temperature of $\Delta T = 0.25$ K and the hysteresis has an amplitude of $T_i - T_m = 8$ K $\gg \Delta T$, we rule out a periodic switching of domains.

For the induced voltage change $\Delta V_{i,m}$ due to domains that remain in the insulating state or metallic state respectively, we find by using Eq. (4):

$$\Delta V_{i,m}(x_0, y_0) \approx -IR_{\text{off}}^2 \frac{D}{L^2} \Delta T \left\langle \frac{dg_{i,m}}{dT}(x_0, y_0) \right\rangle \quad (14)$$

where $\left\langle \frac{dg_{i,m}}{dT}(x_0, y_0) \right\rangle$ is the convolution of the local value of $\frac{dg_{i,m}}{dT}(x_0, y_0)$ with the electron beam induced temperature profile.

In order to obtain an upper estimate for the induced voltage change ΔV , we assume that an area $A_s = \frac{\pi}{4}(\Delta x)^2$ is

homogeneously heated up by the electron beam and that the entire area A_s is either metallic or insulating.

In this case equation 14 reduces to

$$\Delta V_{i,m}(x_0, y_0) \approx -IR_{\text{off}}^2 \frac{D}{L^2} \Delta T A_s \frac{dg_{i,m}}{dT}(x_0, y_0) \quad (15)$$

By considering the resolution of the LTSEM images in the main paper we can estimate $\Delta x \approx 0.5 \mu\text{m}$. We assume a beam induced temperature increase $\Delta T \approx 0.25 \text{ K}$. This value is reasonable. For instance in [33] $\Delta T = 0.2 - 0.4 \text{ K}$ was obtained by considering a totally different LTSEM response mechanism. Finally, we find $\Delta V_i \approx -82 \text{ nV}$ for the insulating phase (which may be neglected due to its smaller magnitude) and $\Delta V_m \approx 19 \mu\text{V}$ for the metallic phase. From this we infer that mainly the metallic phase causes the response ΔV in the LTSEM images.

Note, that the preceding estimate is an upper limit. The signal is reduced, if not all domains within the electron beam induced temperature distribution are in the metallic state. This explains the variation of brightness in the LTSEM images. In addition, current redistribution effects are neglected in the preceding model. But these current redistribution effects can be considerable in a network of fine conducting metallic filaments embedded in an insulating matrix. This might be the reason for the very bright spots in the LTSEM images of Fig. 4 in the main paper.

Computer Model and Additional Simulation Data

In order to simulate the Joule heating in the device, we have developed a computer model, in which the domains are represented by a diamond shaped resistor network [Fig. 12(a)] (like in [21]) consisting of $M \times N$ diamonds. Note, that the program we used is similar to the one used in [13]. For the calculations, the electrical properties as well as the temperature of these resistors are represented by $4 \times M \times N$ dimensional vectors, and for the visualization, we use two dimensional matrices [Fig. 12(b)]. To simulate the IV, the program starts with an input current $I_{\text{in}} = 0$ and a homogenous temperature distribution

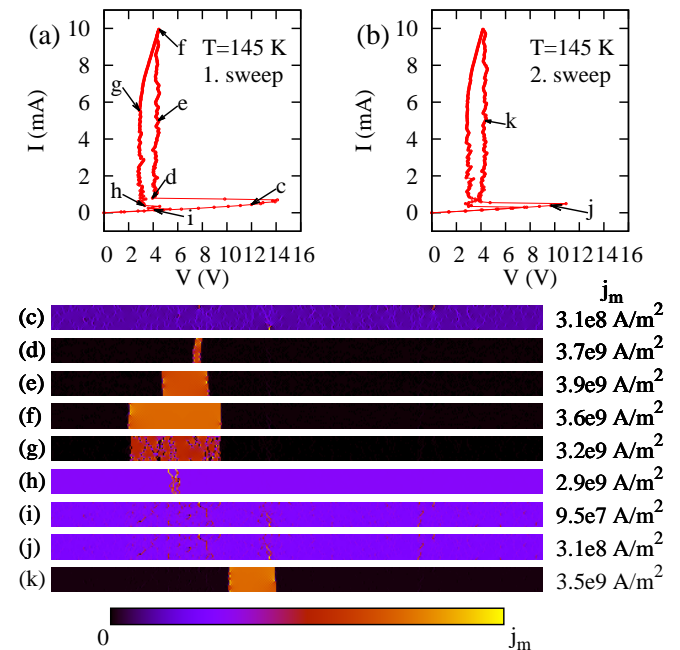


FIG. 8. Simulation of the V_2O_3 device with a base temperature of 145 K. (a) IV of the pristine device. (b) consecutive IV. (c-k) current distribution in the device at different bias points (marked in Fig. a and b).

\vec{T} equals to the base temperature T_b . For every resistor a temperature dependence of the resistance like in the inset of Fig. 4 in the main paper with individual transition temperatures is used. The conductance vector \vec{G} is calculated using the temperature distribution \vec{T} . We have developed an algorithm that creates a set of $4 \times M \times N$ independent Kirchhoff equations corresponding to the re-

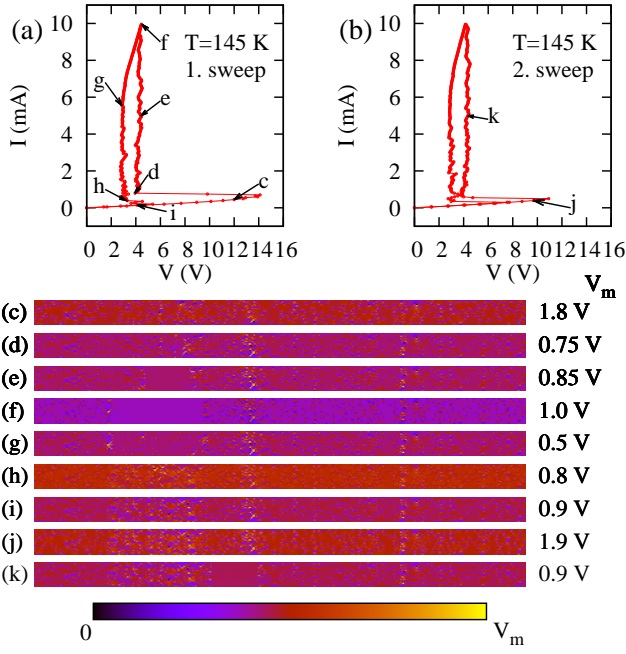


FIG. 9. Simulation of the V_2O_3 device with a base temperature of 145 K. (a) IV of the pristine device. (b) consecutive IV. (c-k) voltage distribution in the device at different bias points (marked in Fig. a and b).

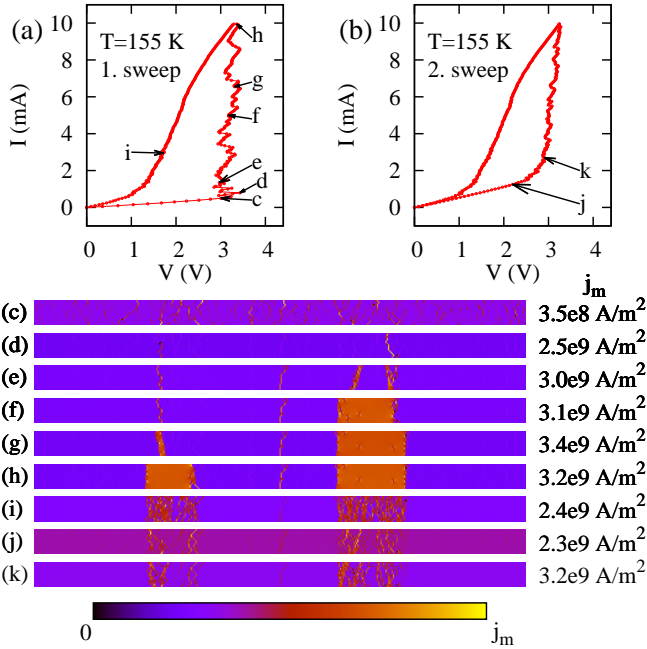


FIG. 10. Simulation of the V_2O_3 device with a base temperature of 155 K. (a) IV of the pristine device. (b) consecutive IV. (c-k) current distribution in the device at different bias points (marked in Fig. a and b)

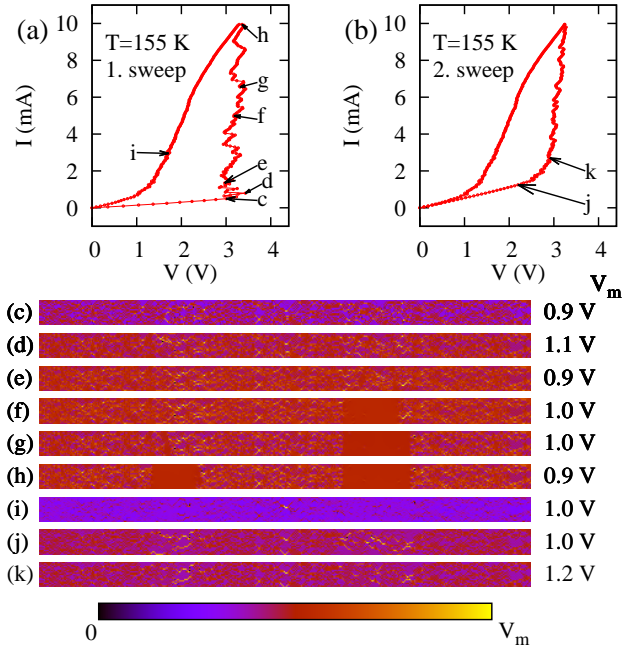


FIG. 11. Simulation of the V_2O_3 device with a base temperature of 155 K. (a) IV of the pristine device. (b) consecutive IV. (c-k) voltage distribution in the device at different bias points (marked in Fig. a and b)

sistor network

$$\mathbf{KM}(\vec{G})\vec{V} = \vec{I}_{in}. \quad (16)$$

We solve for the voltage distribution

$$\vec{V} = \mathbf{KM}^{-1}\vec{I}_{in}, \quad (17)$$

and calculate the current and power distributions

$$\vec{I} = \vec{G} \cdot \vec{V}, \quad \vec{P} = \vec{I} \cdot \vec{V}. \quad (18)$$

With the power distribution the temperature distribution can be recalculated. For the thermal cross coupling (coupling parameter A_c), we consider only coupling between nearest neighbors. For instance, for a network consisting of only 9 resistors (depicted in Fig. 12(c)) we get a thermal coupling equation

$$A_c(T_5 - T_4) + A_c(T_5 - T_2) + \dots + A_s(T_5 - T_b) = P_5, \quad (19)$$

where A_s is the thermal coupling parameter to the cold plate. We have programmed an algorithm that creates the thermal coupling matrix \mathbf{TCM} . The thermal coupling equations can be written as

$$\mathbf{TCM}\vec{T} = \vec{P} + A_s T_b \mathbf{1}. \quad (20)$$

We solve for the temperature distribution

$$\vec{T} = (\mathbf{TCM})^{-1}(\vec{P} + A_s T_b \mathbf{1}) \quad (21)$$

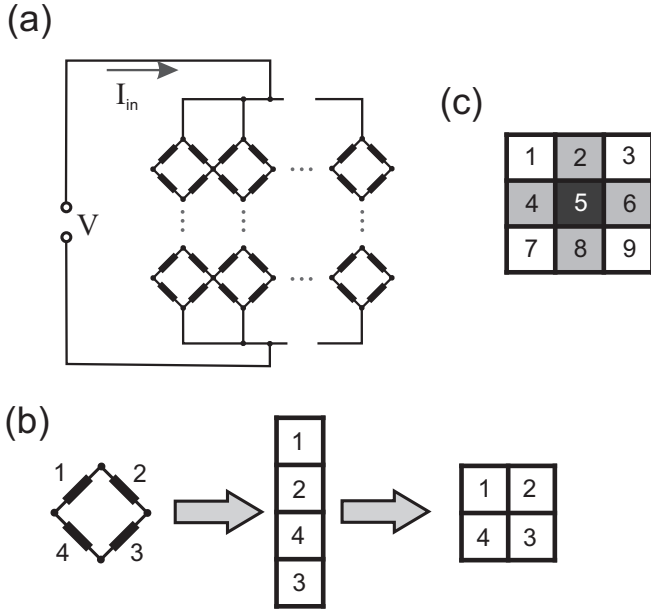


FIG. 12. a) diamond shaped resistor network b) mapping of the resistor network to a vector and a 2D matrix c) thermal cross coupling to nearest neighbors.

We test for convergence by comparing the new temperature distribution with the old one. If the solution is within the convergence criteria, we increment the input current I_{in} and calculate the next bias point, otherwise we recalculate the conductance vector \vec{G} with the new temperature distribution and iterate the program.

The RT curve is simulated in a similar manner. In this case the input current is fixed at a small value and the base temperature is changed by a small increment.

The thermal cross coupling parameter $A_c = 5.0 \cdot 10^{-7} \frac{W}{K}$ was determined by considering the heat flow in the V_2O_3 film, only. The coupling parameter to the cold plate $A_S = 4.25 \cdot 10^{-7} \frac{W}{K}$ was obtained by optimizing the simulation of the IV curves with respect to the measured IV. The thermal conductance of a sapphire block with a ground area of $0.25 \mu m^2$ and a height of $0.5 mm$ is approximately $7.5 \cdot 10^{-8} \frac{W}{K}$. Here, it was assumed that sapphire at a temperature $T = 150 K$ has a thermal conductivity of $150 \frac{W}{m \cdot K}$ [34]. If one takes into account that edge cooling effects were neglected, the thermal coupling parameter A_S is in reasonable agreement with this estimation.

In addition to the temperature distributions presented in the paper the voltage and current distribution was simulated as well. The current distributions depicted in Fig. (8) and (10) are very similar to the temperature distributions presented in the main paper.

The voltage distributions are shown in Fig. (9) and (11).

This work was supported by AFOSR grant number FA9550-12-1-0381. For the computer simulation we used

the linear algebra library Armadillo [35]. We gratefully acknowledge the pioneering work of R. P. Huebener in the field of low temperature scanning electron microscopy.

* stefan.guënon@physics.ucsd.edu

- [1] Z. Yang, C. Ko, and S. Ramanathan, *Annu. Rev. of Mater. Res.* **41**, 337 (2011).
- [2] T. Oka, R. Arita, and H. Aoki, *Phys. Rev. Lett.* **91**, 066406 (2003).
- [3] S. Okamoto, *Phys. Rev. Lett.* **101**, 116807 (2008).
- [4] M. Eckstein, T. Oka, and P. Werner, *Phys. Rev. Lett.* **105**, 146404 (2010).
- [5] F. Heidrich-Meisner, I. González, K. A. Al-Hassanieh, A. E. Feiguin, M. J. Rozenberg, and E. Dagotto, *Phys. Rev. B* **82**, 205110 (2010).
- [6] M. Liu, H. Y. Hwang, H. Tao, A. C. Strikwerda, K. Fan, G. R. Keiser, A. J. Sternbach, K. G. West, S. Kittiwatanakul, J. Lu, S. A. Wolf, F. G. Omenetto, X. Zhang, K. A. Nelson, and R. D. Averitt, *Nature* **487**, 345 (2012).
- [7] C. Berglund, *IEEE Trans. Electron Devices* **16**, 432 (1969).
- [8] J. Duchene, M. Terrailon, P. Pailly, and G. Adam, *Appl. Phys. Lett.* **19**, 115 (1971).
- [9] J. R. Clem and R. P. Huebener, *J. Appl. Phys.* **51**, 2764 (1980).
- [10] R. Gross and D. Koelle, *Rep. Prog. Phys.* **57**, 651 (1994).
- [11] J. Kim, C. Ko, A. Frenzel, S. Ramanathan, and J. E. Hoffman, *Appl. Phys. Lett.* **96**, 213106 (2010).
- [12] C. Grygiel, A. Pautrat, W. Prellier, and B. Mercey, *EPL (Europhysics Letters)* **84**, 47003 (2008).
- [13] A. Sharoni, J. G. Ramírez, and I. K. Schuller, *Phys. Rev. Lett.* **101**, 026404 (2008).
- [14] W. Bao, C. Broholm, G. Aeppli, S. A. Carter, P. Dai, T. F. Rosenbaum, J. M. Honig, P. Metcalf, and S. F. Trevino, *Phys. Rev. B* **58**, 12727 (1998).
- [15] A. Tanaka, *J. Phys. Soc. Jpn.* **71**, 1091 (2002).
- [16] P. Pfalzer, G. Obermeier, M. Klemm, S. Horn, and M. L. denBoer, *Phys. Rev. B* **73**, 144106 (2006).
- [17] H. Schuler, S. Klimm, G. Weissmann, C. Renner, and S. Horn, *Thin Solid Films* **299**, 119 (1997).
- [18] A. Volkov and M. Kogan, *Sov. Phys. Usp.* **11**, 881 (1969).
- [19] A. V. Gurevich and R. G. Mints, *Rev. Mod. Phys.* **59**, 941 (1987).
- [20] B. Fisher, *J. Phys. C* **8**, 2072 (1975).
- [21] A. Shekhawat, S. Papanikolaou, S. Zapperi, and J. P. Sethna, *Phys. Rev. Lett.* **107**, 276401 (2011).
- [22] R. Eichele, L. Freytag, H. Seifert, R. P. Huebener, and J. R. Clem, *J. Low Temp. Phys.* **52**, 449 (1983).
- [23] D. Doenitz, R. Kleiner, D. Koelle, T. Scherer, and K. F. Schuster, *Applied Physics Letters* **90**, 252512 (2007).
- [24] E. Spenke, *Electrical Engineering (Archiv für Elektrotechnik)* **30**, 728 (1936).
- [25] E. Spenke, *Wissenschaftliche Veröffentlichungen aus den Siemens-Werken* **15**, 92 (1936).
- [26] H. B. Wang, S. Guënon, J. Yuan, A. Iishi, S. Arisawa, T. Hatano, T. Yamashita, D. Koelle, and R. Kleiner, *Phys. Rev. Lett.* **102**, 017006 (2009).
- [27] H. B. Wang, S. Guënon, B. Gross, J. Yuan, Z. G. Jiang, Y. Y. Zhong, M. Grünzweig, A. Iishi, P. H. Wu, T. Hatano, D. Koelle, and R. Kleiner, *Phys. Rev. Lett.*

- 105**, 057002 (2010).
- [28] S. Guénon, M. Grünzweig, B. Gross, J. Yuan, Z. G. Jiang, Y. Y. Zhong, M. Y. Li, A. Iishi, P. H. Wu, T. Hatano, R. G. Mints, E. Goldobin, D. Koelle, H. B. Wang, and R. Kleiner, *Phys. Rev. B* **82**, 214506 (2010).
- [29] B. Gross, S. Guénon, J. Yuan, M. Y. Li, J. Li, A. Iishi, R. G. Mints, T. Hatano, P. H. Wu, D. Koelle, H. B. Wang, and R. Kleiner, *ArXiv e-prints* (2012), arXiv:1206.6275 [cond-mat.supr-con].
- [30] J.-G. Zhang and P. Eklund, *J. Mater. Res.* (1993).
- [31] H. Busch, *Annalen der Physik* **64**, 401 (1921).
- [32] M. Büttiger and R. Landauer, in *Nonlinear Phenomena at Phase Transitions and Instabilities*, edited by T. Riste (Plenum, New York/London, 1982) p. 111.
- [33] C. Gürlich, S. Scharinger, M. Weides, H. Kohlstedt, R. G. Mints, E. Goldobin, D. Koelle, and R. Kleiner, *Phys. Rev. B* **81**, 094502 (2010).
- [34] Y. S. Touloukian and E. H. Buyco, *Thermal Conductivity*, Vol. 1 and 2 (Plenum Press, New York, 1970).
- [35] C. Sanderson, *Armadillo: An Open Source C++ Linear Algebra Library*, Tech. Rep. (NICTA, Australia, 2010).